Structural health monitoring of a cable-stayed bridge using wireless smart sensor technology: data analyses

Soojin Cho[1], Hongki Jo[2], Shinae Jang[2], Jongwoong Park[1], Hyung-Jo Jung[1]*, Chung-Bang Yun[1], Billie F. Spencer, Jr.[2] and Ju-Won Seo[3]

[1]*Department of Civil and Environmental Engineering, KAIST, 373-1 Guseong-dong, Yuseong-gu, Daejeon 305-701, South Korea*
[2]*Department of Civil and Environmental Engineering, University of Illinois at Urbana-Champaign, 205 North Mathews Avenue, Urbana, IL 61801, USA*
[3]*Long Span Bridge Research Team, Hyundai Instititue of Construction Technology, 102-4 Mabook-dong, Giheung-gu, Yongin, Gyounggi-do 449-716, South Korea*

(Received November 13, 2009, Accepted March 4, 2010)

Abstract. This paper analyses the data collected from the 2nd Jindo Bridge, a cable-stayed bridge in Korea that is a structural health monitoring (SHM) international test bed for advanced wireless smart sensors network (WSSN) technology. The SHM system consists of a total of 70 wireless smart sensor nodes deployed underneath of the deck, on the pylons, and on the cables to capture the vibration of the bridge excited by traffic and environmental loadings. Analysis of the data is performed in both the time and frequency domains. Modal properties of the bridge are identified using the frequency domain decomposition and the stochastic subspace identification methods based on the output-only measurements, and the results are compared with those obtained from a detailed finite element model. Tension forces for the 10 instrumented stay cables are also estimated from the ambient acceleration data and compared both with those from the initial design and with those obtained during two previous regular inspections. The results of the data analyses demonstrate that the WSSN-based SHM system performs effectively for this cable-stayed bridge, giving direct access to the physical status of the bridge.

Keywords: wireless smart sensor network; cable-stayed bridge; structural health monitoring; modal identification; cable tension estimation.

1. Introduction

Jang *et al*. (2010) describes field deployment of structural health monitoring (SHM) system using wireless smart sensor technology on a cable-stayed bridge in Korea (the 2nd Jindo Bridge). A total of 70 wireless smart sensor nodes are installed with high spatial density on the bridge, facilitating measurements of 3-axis acceleration underneath of the deck, on two pylons, and on the cables. Using two base stations, measurement has been carried out during the past 4 months using an autonomous monitoring system based on the SHM framework proposed by Rice *et al.* (2010). Overall performance of the system has been evaluated in terms of hardware durability, software stability, power consumption and harvesting (Jang *et al*. 2010).

*Corresponding Author, Associate Professor, E-mail: hjung@kaist.ac.kr

The next generation of SHM systems must move from the *nice-to-have* to the *need-to-have* paradigm that is essential and beneficial for structure operation and maintenance (Fujino *et al.* 2009). To date, wireless smart sensing technology has been studied in depth by many researchers for monitoring large civil infrastructures; however, only a few full-scale deployments have been realized, most of which were for demonstration purposes only. For example, Weng *et al*. (2008) reported a monitoring campaign to determine the modal properties of the Gi-Lu cable-stayed Bridge in Taiwan using 12 wireless sensing units interfaced to velocity meters. Various sensor configurations (i.e., on the deck only or both on the deck and cables) were considered to identify the modal properties of the global structure, as well as cable tension forces. Pakzad *et al*. (2008) instrumented a total of 64 wireless sensor nodes on the deck, one of the towers, and several cables of the Golden Gate Bridge. A pipeline multi-hop communication protocol was successful to collect the measured data, which was utilized to evaluate the performance of the wireless sensor network, as well as to identify modal properties of the bridge. Both of these efforts were short-term demonstration projects.

This paper assesses the performance of the wireless SHM system installed at the 2nd Jindo Bridge by analyzing the measured acceleration data. This cable-stayed bridge in Korea is a structural health monitoring (SHM) international test bed for advanced wireless smart sensors network (WSSN) technology. First, a finite element (FE) model is constructed based on an in-depth study of the detailed drawings and design documents, and validated using the acceleration data from the existing wired monitoring system on the bridge. The acceleration data collected from the current wireless smart sensor network (WSSN) at two base stations (Haenam-side and Jindo-side) are subsequently analyzed. Two output-only modal identification (ID) methods are used to extract the modal properties of the bridge from the ambient acceleration data of the deck and the pylons. The extracted modal properties from both modal ID methods are validated by comparing with each other and with those from the FE analysis. Tension forces are estimated on 10 of the bridge's stay cables using data collected from the sensor nodes mounted on the cables. The estimated tension forces are compared both with those used in the initial design and with those obtained during the regular inspections in 2007 and 2008. Finally, a discussion is provided regarding the efficacy of the monitoring strategy utilizing the WSSN for comprehensive SHM of the cable-stayed bridge.

2. Finite element model of Jindo Bridge

2.1 Construction of finite element model

Prior to the sensor deployment, a finite element (FE) model of the 2nd Jindo Bridge is constructed for validation of the analysis results of the measured data based on detailed drawings and design documents. A commercial structural analysis software, MIDAS/CIVIL (MidasIT 2009), is used. The bridge's main box girder is modeled by 128 frame elements with 6 different sectional properties. Additional masses are appended to the girder to represent the pavement, guard rails, water supply pipes, curbs and diaphragms. Each of two pylons is modeled by 110 frame elements with 7 different sectional properties. The spread footings of the pylons are on the stiff rock and thus modeled as fixed boundary conditions. The cables are modeled by truss elements with Ernst equivalent elastic moduli to consider the nonlinear effect caused by self-weight of cables with resulting tension forces and sag (Ernst 1965). Fig. 1 shows the resulting FE model of the 2nd Jindo Bridge.

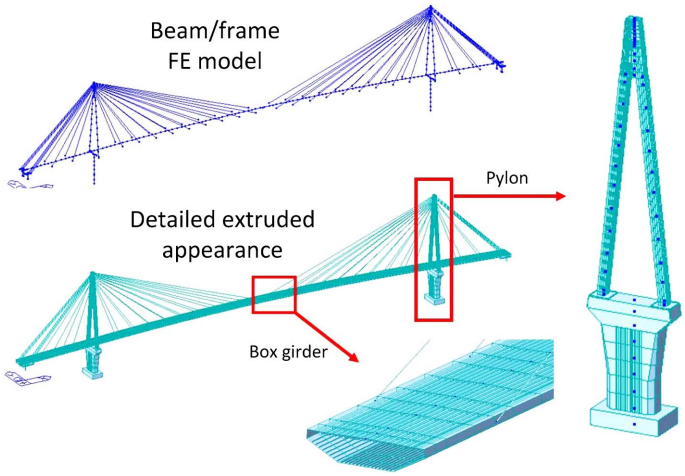

Fig. 1 FE model of the 2nd Jindo Bridge constructed using MIDAS/CIVIL

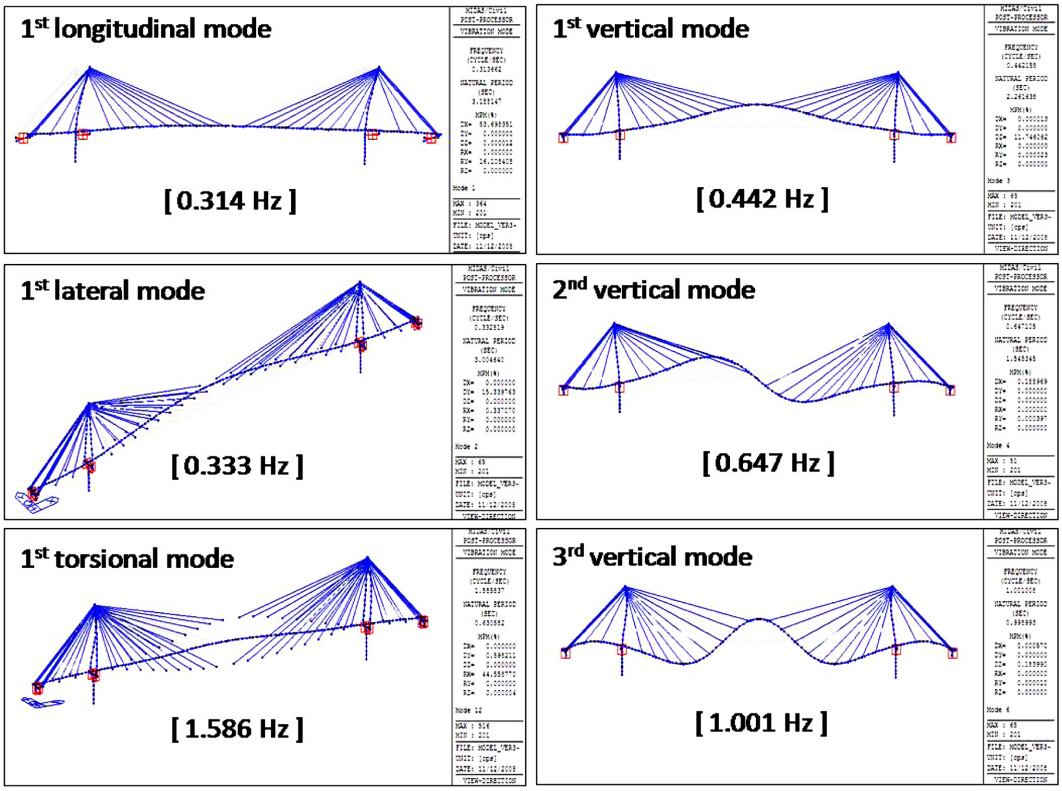

Fig. 2 Mode shapes and natural frequencies of the 2nd Jindo Bridge from the FE analysis

2.2 Validation of the finite element model

A preliminary validation of the FE model is achieved by comparing the computed modal properties with those extracted from acceleration responses measured in 2007 using the existing

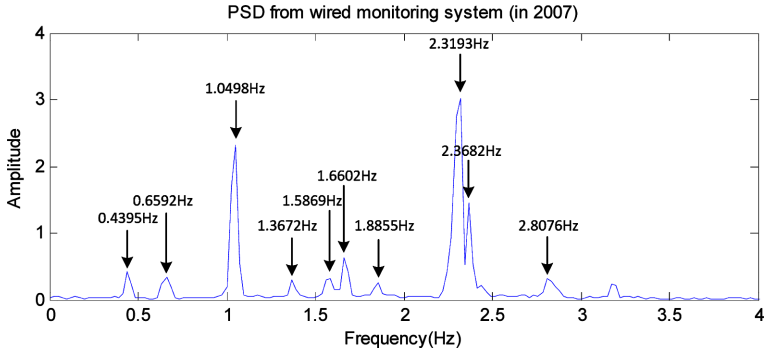

Fig. 3 PSD of a vertical acceleration record collected in 2007 using the existing wired monitoring system

wired monitoring system. Fig. 2 shows the first six mode shapes evaluated from the FE model, including longitudinal, lateral, vertical and torsional modes. The first 10 natural frequencies of the vertical modes are obtained as 0.442, 0.647, 1.001, 1.247, 1.349, 1.460, 1.586, 2.115, 2.139 and 2.561 Hz. Fig. 3 shows the power spectral density (PSD) of a vertical acceleration record, which contains vertical and torsional mode information, measured at a quarter span of the deck in 2007. The first 3 peak frequencies (i.e., 0.440, 0.659 and 1.050 Hz) are in very good agreements with the FE analysis results, while the higher modal frequencies are larger than the FE results. The differences in these higher modes are within 16%, which shows the general validity of the FE model; however, updating of the FE model may increase the efficacy of the model for comprehensive SHM of the bridge.

3. Wireless smart sensor network and measured data

3.1 Wireless smart sensor network

The 2nd Jindo Bridge at the southern tip of the Korean peninsula has been established as an international SHM test bed for advanced wireless smart sensor network (WSSN) technology (see Fig. 4). This trilateral collaborative research effort between Korea (KAIST), the USA (University of Illinois at Urbana-Champaign), and Japan (University of Tokyo) constitutes the largest deployment of wireless smart sensors to date for monitoring civil infrastructure. A detailed description of this test bed can be found in Rice *et al.* (2010) and Jang *et al.* (2010); for completeness, a brief synopsis is provided here.

A total of 70 wireless smart sensor nodes (leaf nodes) are installed on the 2nd Jindo Bridge. To facilitate efficient data collection, the 70 nodes are divided into two sub-networks: 37 nodes on the Haenam-side and 33 nodes on the Jindo-side, as shown in Fig. 5. 49 nodes are installed under the deck, with additional six nodes on the two pylons and 15 nodes on the stay cables. Each leaf node is comprised of an Imote2, a multi-scale sensor board including a tri-axial accelerometer, and a battery board with three D-cell batteries; the components are all housed in environmentally hardened plastic enclosures. Two base stations are located at the tops of two pylon bases of the 1st Jindo Bridge adjacent to the 2nd Jindo Bridge to secure the line-of-sight wireless transmission path between leaf nodes and gateway nodes of base stations. Each base station is composed of an

Fig. 4 1st (right) and 2nd (left) Jindo Bridges (Jang *et al*. 2010)

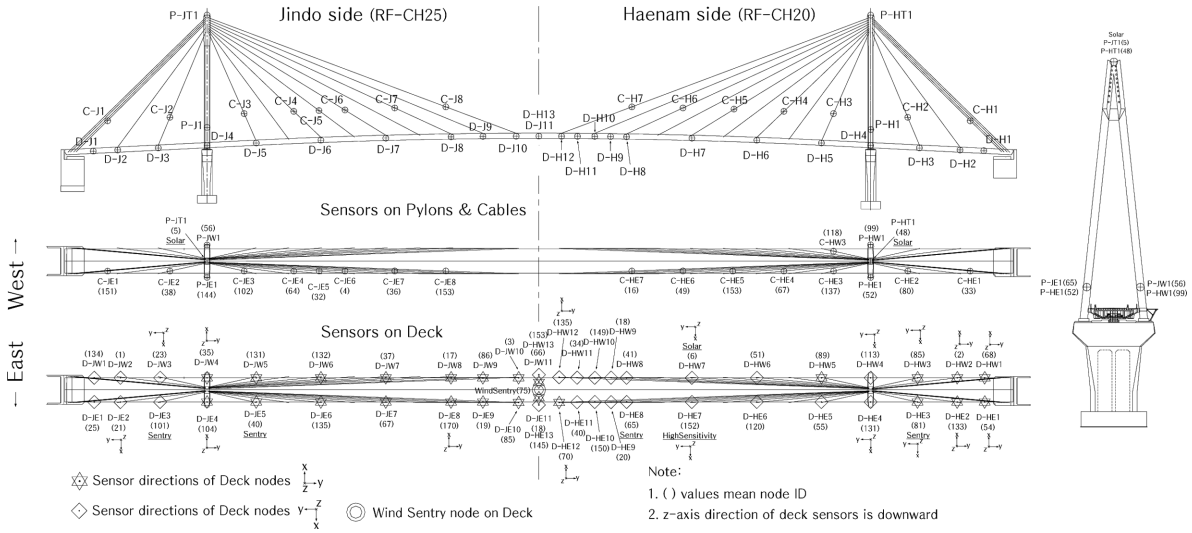

Fig. 5 Sensor locations (Jang *et al*. 2010)

industrial-purpose PC, a gateway node, and an ADSL modem to connect the PC to the internet. The gateway node broadcasts commands to the leaf nodes in its sub-network, collects measured data, and stores it on the PC. For efficient management of the battery power, ordinary leaf nodes are normally in a deep-sleep state, periodically waking to listen for network alerts. Such alerts are provided by the *Sentry* nodes, which are programmed to wake up and measure the data at predefined times; when the measured wind velocity and acceleration responses exceed prescribed threshold levels the network is alerted and network-wide data collection is initiated. The wind speed threshold is set at 3 m/s, whereas the acceleration threshold is set at 10 mg during normal operation. For each network-wide measurement instance, 500 seconds of data is taken using a 10-Hz sampling rate (i.e., 5000 samples); anti-aliasing filters are employed with a 4-Hz cutoff frequency (Rice *et al*. 2010).

3.2 Measured acceleration data

The coordinate system of the global structure and cables is priorly determined in Fig. 6 to help readers for direction of the measured data. Fig. 7 shows examples of the ambient acceleration data

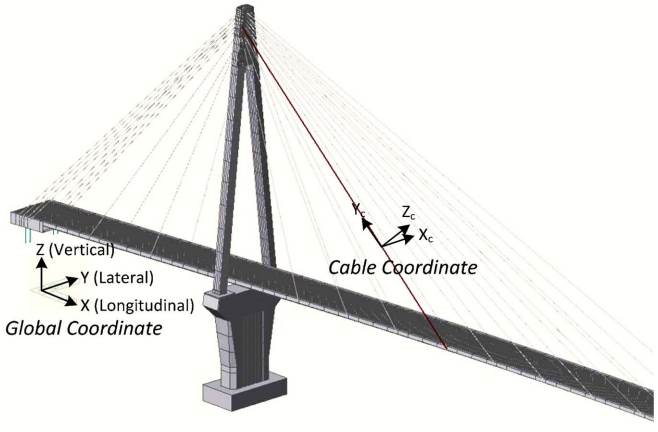

Fig. 6 Coordinate system for global structure and cables

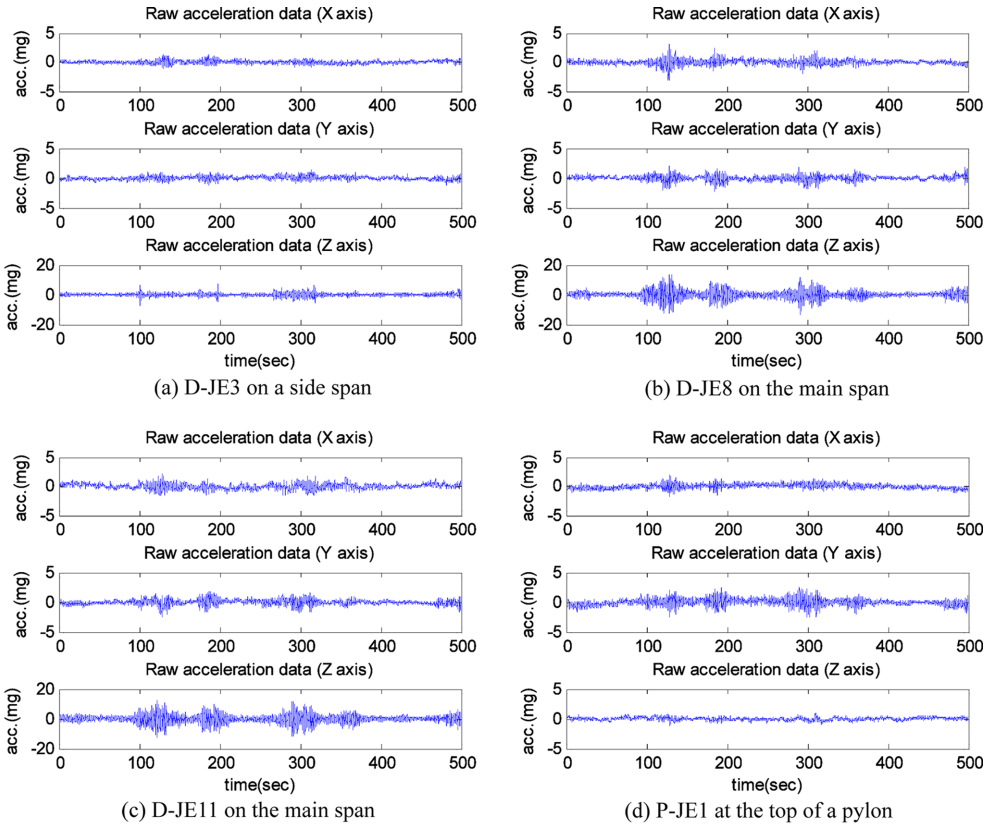

(a) D-JE3 on a side span

(b) D-JE8 on the main span

(c) D-JE11 on the main span

(d) P-JE1 at the top of a pylon

Fig. 7 Examples of measured acceleration data on the deck and a pylon (Jindo-side, on 9/11/2009)

measured on the deck and the pylons in the three global coordinate directions. The amplitudes of the acceleration due to automobile traffic on the bridge are found to be large enough for mode extraction, especially for the vertical modes (*Z*-axis). Fig. 8 shows examples of the ambient acceleration data measured on 2 cables. Similar to the deck vibration, the cable vibration in Z_c-axis (usually

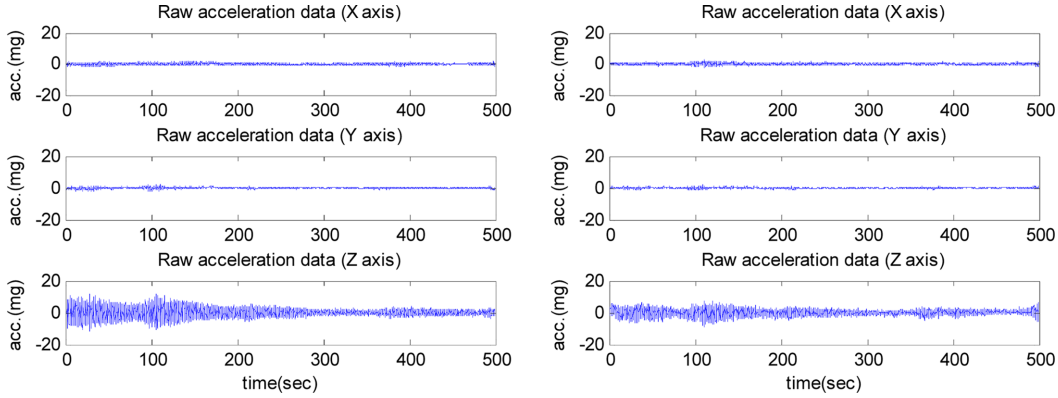

(a) C-JE7 on Cable JC13 (b) C-JE8 on Cable JC15

Fig. 8 Examples of measured acceleration data on cables (Jindo-side, on 9/11/2009)

referred as "vertical" or "in-plane" vibration in many literatures) is much larger than the other vibration components in X_c- and Y_c-axis. The cable-vibration amplitudes are also found to be sufficiently large for mode extraction, which will be used for estimation of the cable tension forces as described in a subsequent section.

4. Output-only modal identification

Modal properties such as natural frequencies, mode shapes and modal damping ratios play key roles for SHM of bridges. For example, they are used for evaluating the structural integrity (Koo *et al*. 2008), assessing aerodynamic stability (Jain *et al.* 1998), calibrating the baseline finite element model (Yun 2001), and vibration control of deck and cables (Koshimura *et al*. 1994, Li *et al*. 2007). To analyze the ambient (or operational) acceleration data excited by ambient sources, such as wind and traffic, output-only modal identification methods are required. The output-only modal identification methods are based on the assumption that input is broadband Gaussian random process. In this study, two output-only modal identification methods are employed using the ambient vibration data. They are the frequency domain decomposition (FDD) and stochastic subspace identification (SSI) methods. For completeness, a brief outline of the methods is included in this section.

4.1 Theory of output-only modal identification methods

4.1.1 Frequency domain decomposition method

The FDD method (Brinker *et al.* 2001) starts by constructing and decomposing the PSD matrix for the measured data via the singular value decomposition (SVD)

$$\mathbf{S}_{\mathbf{yy}}(\omega) = \mathbf{U}(\omega)\Sigma(\omega)\mathbf{V}^{T}(\omega) \tag{1}$$

where $\mathbf{y}$ is the measurement vector; $\mathbf{S}_{\mathbf{yy}}(\omega)$ is the PSD matrix; Σ is the diagonal matrix containing the singular values ($\sigma_i(\omega)$) in descending order; and $\mathbf{U}$ and $\mathbf{V}$ are unitary matrices containing the left and right singular vectors. Due to the symmetry of $\mathbf{S}_{\mathbf{yy}}(\omega)$, $\mathbf{U}$ is equal to $\mathbf{V}$. The magnitudes of the singular

values indicate the relative level of vibration at the corresponding frequencies. The peaks in the plot of the 1st singular value versus frequency can be interpreted as natural frequencies of the structure, while the corresponding 1st singular vectors at these frequencies can be interpreted as the associated mode shapes. Thus, the natural frequencies can be estimated by the conventional peak picking method using the 1st singular value function.

4.1.2 Stochastic subspace identification method

The SSI method (Overshcee and De Moor 1993, Peeters and De Roeck 1999) starts from the state space representation for the equations of motion assuming a linear time-invariant system

$$\begin{aligned} \mathbf{x}(k+1) &= \mathbf{A}\mathbf{x}(k) + \mathbf{w}(k) \\ \mathbf{y}(k) &= \mathbf{C}\mathbf{x}(k) + \mathbf{v}(k) \end{aligned} \tag{2}$$

Where $\mathbf{x}(k)$ is the state vector at time $t = k\Delta t$; $\mathbf{y}$ is the observation vector at time $t = k\Delta t$; $\mathbf{A}$ is the discrete state matrix; $\mathbf{C}$ is the observation matrix; and $\mathbf{w}(k)$ and $\mathbf{v}(k)$ are the process and measurement noises which are assumed to be uncorrelated Gaussian random sequences.

The cross correlation matrix of the observation can be written as

$$\mathbf{R}_k = E[\mathbf{y}(k+i)\mathbf{y}(i)^T] = \mathbf{C}\mathbf{A}^{k-1}E[\mathbf{x}(i+1)\mathbf{y}(i)^T] = \mathbf{C}\mathbf{A}^{k-1}\mathbf{G} \tag{3}$$

Then, the Hankel matrix can be composed of a series of the cross correlation matrices, which can be decomposed into an observability matrix ($\mathcal{O}_{n_1}$) and an extended controllability matrix ($\mathcal{C}_{n_2}^{ext}$) as

$$\begin{aligned} \mathbf{H}_{n_1,n_2} &= \begin{bmatrix} \mathbf{R}_1 & \cdots & \mathbf{R}_{n_2} \\ \vdots & \ddots & \vdots \\ \mathbf{R}_{n_1} & \cdots & \mathbf{R}_{n_1+n_2-1} \end{bmatrix} = \begin{bmatrix} \mathbf{CG} & \cdots & \mathbf{CA}^{n_2-1}\mathbf{G} \\ \vdots & \ddots & \vdots \\ \mathbf{CA}^{n_1-1}\mathbf{G} & \cdots & \mathbf{CA}^{n_1+n_2-2}\mathbf{G} \end{bmatrix} \\ &= \begin{bmatrix} \mathbf{C} \\ \vdots \\ \mathbf{CA}^{n_1-1} \end{bmatrix} \begin{bmatrix} \mathbf{G} & \cdots & \mathbf{A}^{n_2-1} \end{bmatrix} = \mathcal{O}_{n_1}\mathcal{C}_{n_2}^{ext} \end{aligned} \tag{4}$$

If $\mathbf{H}_{n_1,n_2}$ is decomposed by SVD as

$$\mathbf{H}_{n_1,n_2} = \begin{bmatrix} \mathbf{U}_1 & \mathbf{U}_2 \end{bmatrix} \begin{bmatrix} \mathbf{\Sigma}_1 & 0 \\ 0 & 0 \end{bmatrix} \begin{bmatrix} \mathbf{V}_1 \\ \mathbf{V}_2 \end{bmatrix}^T \approx \mathbf{U}_1\mathbf{\Sigma}_1\mathbf{V}_1^T \tag{5}$$

The observability matrix can be obtained as

$$\mathcal{O}_{n_1} = \mathbf{U}_1\mathbf{\Sigma}_1^{1/2} = \mathcal{O}_{n_1-1} \begin{bmatrix} \mathbf{C} \\ \mathbf{CA} \\ \vdots \\ \mathbf{CA}^{n_1-2} \\ \mathbf{CA}^{n_1-1} \end{bmatrix} \mathcal{O}_{n_1-1}^{\uparrow} \tag{6}$$

From Eq. (6), the following relationship can be established, from which the discrete state matrix $\mathbf{A}$ can be obtained using the pseudo-inverse technique

$$\mathcal{O}_{n_1-1}^{\uparrow} = \mathcal{O}_{n_1-1}\mathbf{A} \tag{7}$$

From the discrete state matrix **A** the eigenvalue (λ_i) and eigenvector (ψ_i) can be obtained, from which the natural frequencies (ω_i) and mode shapes (ϕ_i) can be obtained from the following relationships

$$\lambda_{C_i}, \lambda_{C_i}^* = -\xi_i \omega_i \pm j\omega_i \sqrt{1-\xi_i^2}$$
$$\phi_i = \mathbf{C}\psi_i \tag{8}$$

where $\lambda_{C_i} = \dfrac{\ln(\lambda_i)}{\Delta t}$ is the i^{th} eigenvalue of continuous system; Δt is the sampling time; ξ_i is the modal damping ratio; and asterisk (*) denotes complex conjugate.

SSI requires the system order n to be determined *a priori*. In this study, a stabilization chart is used to find a suitable system order with the criterions provided by Yi and Yun (2004). The stabilization chart shows the stable modes as a function of increasing system order p. To construct the stabilization chart, noise modes are identified and discarded for each system order p. To the end, the natural frequencies, modal damping ratios, and modal assurance criterion (MAC) values of the modes for the system of order p with those from the system of order p-1 (adjacent system orders) is estimated. First, mode for which the modal damping ratio is determined to be larger than 0.5 is classified as a noise mode and discarded. Among the non-noise modes, stable modes are classified when the normalized differences of natural frequencies, and modal damping ratios with the system at the system order p-1 are less than 0.01 and 0.2, respectively, and when MAC value is larger than 0.95.

4.2 Results of modal analysis

4.2.1 Identified modal properties from individual WSSN

Modal analyses are carried out on the two sets of data obtained from Haenam- and Jindo-side WSSNs using the two previously described output-only modal identification methods. Because the WSSNs are not synchronized to each other during the measurement, the data from each WSSN are analyzed independently, and then combined subsequently. To obtain the PSD matrix for the FDD method, each 5000 point acceleration data record is processed using a 1024 point FFT, employing 50% overlap and a Hanning window using the Matlab CPSD command.

Fig. 9 shows the stabilization charts for SSI plotted along with the 1st singular values of FDD. Using SSI, 12 stable modes and 3 noise modes (NC1-3) are identified at a high system order (n>60) in the frequency range of 0-3 Hz. The resonant frequencies are found to have good agreements with the peak frequencies from FDD. Table 1 gives descriptions of the identified modes; Tables 2 and 3 and Figs. 10 and 11 show the natural frequencies and mode shapes determined by SSI and FDD, respectively, from the two WSSNs. The results from different modal identification methods are found to be consistent to each other. Note that the noise modes can be attributed to two malfunctioning leaf nodes (D-HE12 and D-JE7 - see Fig. 5) with unexpected noises at 0.82 Hz, 1.64 Hz and 2.46 Hz.

Several modes (DL1, DV2, DT1 and PB1 - see Table 1) are found undetected by FDD. In Figs. 10 and 11, some mode shapes extracted by FDD show un-smooth shapes at a few sensor locations, while those by SSI are generally smooth. If longer acceleration records were collected, the modal properties of both FDD and SSI would be in better agreement. However, the SSI method can reduce significantly the amount of data, and thus transmission time, processed in a large-scale WSSN. The present results show that SSI with a system order greater than 60 yields reasonable results.

In Table 2, the identified natural frequencies are compared with those obtained from both the wired monitoring system and the FE analysis. The identified natural frequencies show excellent agreements

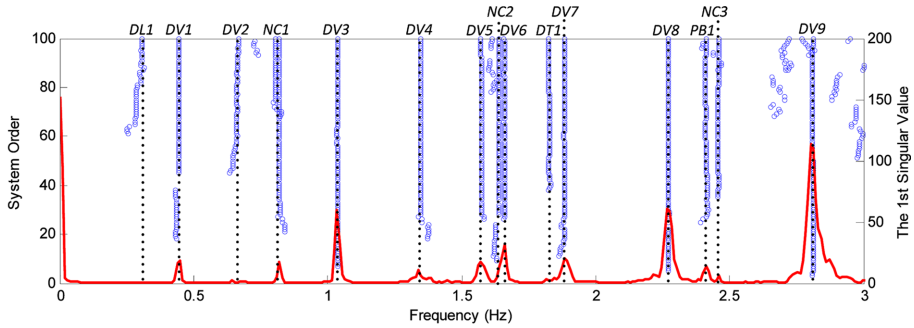

(a) Haenam-side WSSN (on 9/8/2009)

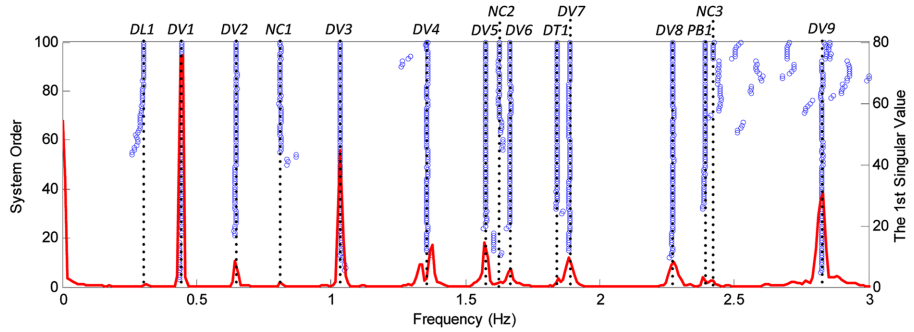

(b) Jindo-side WSSN (on 9/11/2009)

Fig. 9 Comparison of stabilization chart of SSI with the 1st singular values of FDD

Table 1 Modes extracted by output-only modal identification (0-3Hz)

No.	Name	Main member	Mode Shape
1	DL1	Deck	1st longitudinal mode
2	DV1	Deck	1st vertical mode
3	DV2	Deck	2nd vertical mode
4	DV3	Deck	3rd vertical mode
5	DV4	Deck	4th vertical mode
6	DV5	Deck	5th vertical mode
7	DV6	Deck	6th vertical mode
8	DT1	Deck	1st torsional mode
9	DV7	Deck	7th vertical mode
10	DV8	Deck	8th vertical mode
11	PB1	Pylon	1st bending mode
12	DV1	Deck	9th vertical mode
-	NC1-NC3	-	Noise mode from two malfunctioning nodes

with the frequencies obtained from the wired monitoring system in 2007. The results are also found to be in good agreement with the FE analysis through the 3rd vertical mode, while those for the higher modes are generally larger than the FE results. However, the differences are found to be within 16%.

Table 2 Natural frequencies from SSI and FDD (Haenam-side on 9/8/2009, Jindo-side on 9/11/2009)

No.	Modes	SSI (Hz)		FDD (Hz)		Wired monitoring system (Hz)	FE analysis (Hz)
		Haenam-side	Jindo-side	Haenam-side	Jindo-side		
1	DL1	0.2998	0.2985	-	-	-	0.3137
2	DV1	0.4347	0.4380	0.4492	0.4492	0.4395	0.4422
3	DV2	0.6619	0.6439	-	0.6445	0.6592	0.6471
4	DV3	1.0371	1.0364	1.0352	1.0352	1.0498	1.0010
5	DV4	1.3481	1.3555	1.3379	1.3379	1.3672	1.2472
6	DV5	1.5755	1.5759	1.5723	1.5723	1.5869	1.3490
7	DV6	1.6618	1.6660	1.6602	1.6699	1.6602	1.4596
8	DT1	1.8278	1.8410	-	-	-	1.7888
9	DV7	1.8844	1.8860	1.8848	1.8848	1.8555	1.5858
10	DV8	2.2712	2.2731	2.2656	2.2754	2.3193	2.1154
11	PB1	2.4107	2.3890	2.4121	-	2.3682	2.1392
12	DV9	2.8127	2.8266	2.8027	2.8320	2.8076	2.5612

4.2.2 Combination of modes from two sensor networks

The modal properties from each WSSN are combined to provide the global information for SHM. To construct the global mode shapes, least-square method is applied to knit the modes together at the four overlapped reference nodes at mid-span (see Fig. 12). Examples of the combined mode shapes are compared with those from the FE analysis in Fig. 13. The MAC values of 0.943-0.986 between the respective modes demonstrate the excellent agreement in the results, reinforcing the exceptional performance of the WSSN. The software is currently under development for synchronization of two separated base stations and expected to be implemented on the 2nd Jindo Bridge in the near future. The decentralized data aggregation (Sim *et al*. 2010) and decentralized processing (Jeong and Koh 2009) appropriate to monitoring of the cable-stayed bridge is destined to be implemented with the help of one base station as well.

5. Estimation of cable tension forces

5.1 Description of cable properties

The 2nd Jindo Bridge has a total of 60 parallel wire strand (PWS) stay cables. The bridge is symmetric along the longitudinal as well as the lateral directions. Each pylon holds 30 cables; 15 cables on each of east and west sides. The cables are categorized into 4 groups with different cross sections (i.e.: ϕ7×139, ϕ7×109, ϕ7×73, and ϕ7×151) as shown in Fig. 14. The above designations indicate the number of 7 mm diameter steel wires in a cable. High-damping rubber dampers are installed on cable anchors to reduce the wind-induced cable vibration.

Among the 15 cables instrumented by wireless smart sensor nodes, 10 east-side cables are selected to estimate the tension forces due to the collocation of wired sensors as well as their large tension levels, as shown in Fig. 14. Table 3 shows the general properties of the cables. The effective lengths of the cables are obtained from the work by Park *et al*. (2008). Note that the leaf nodes

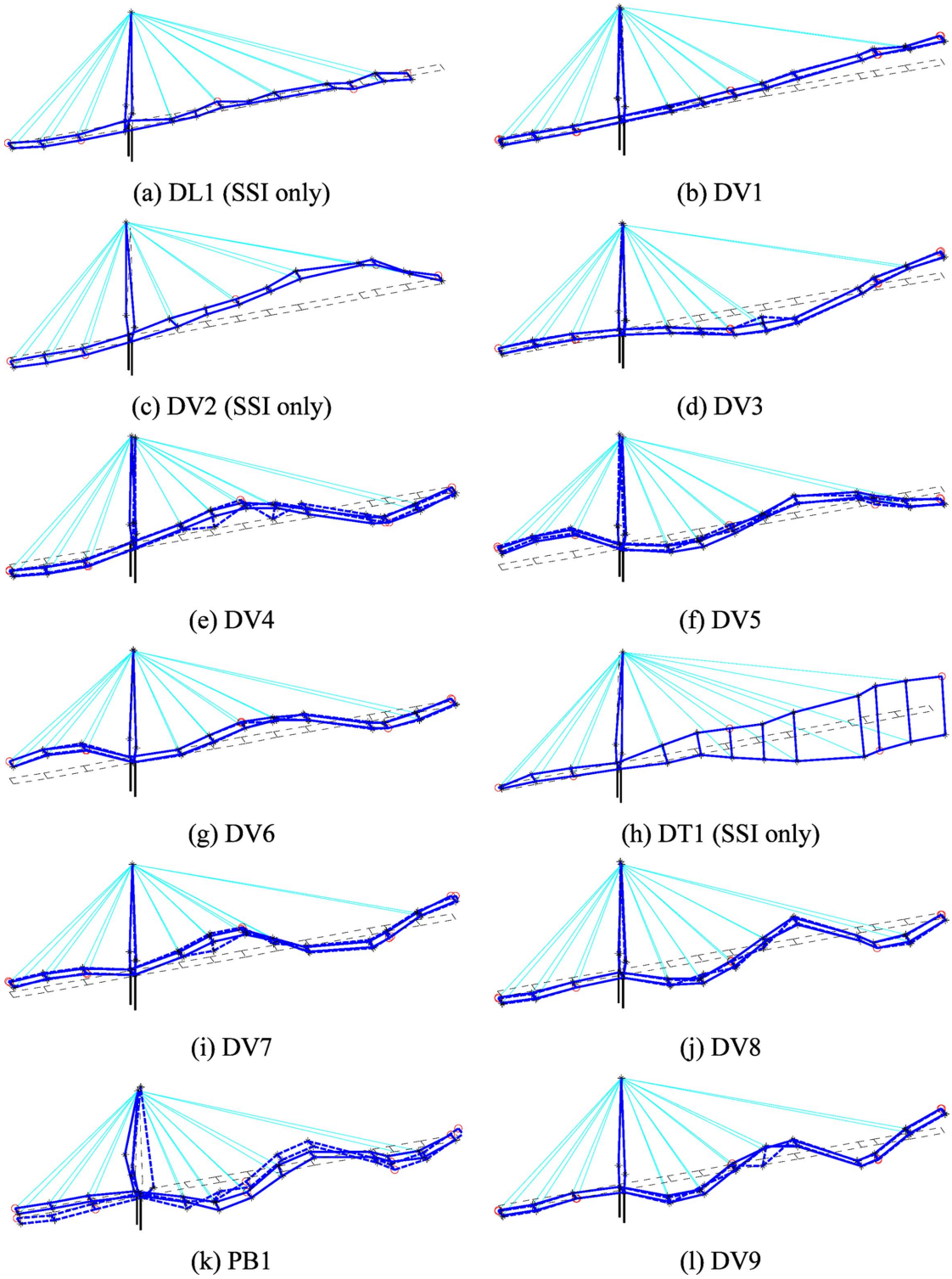

Fig. 10 Mode shapes from SSI (solid line) and FDD (dashed line): Haenam-side, on 9/8/2009

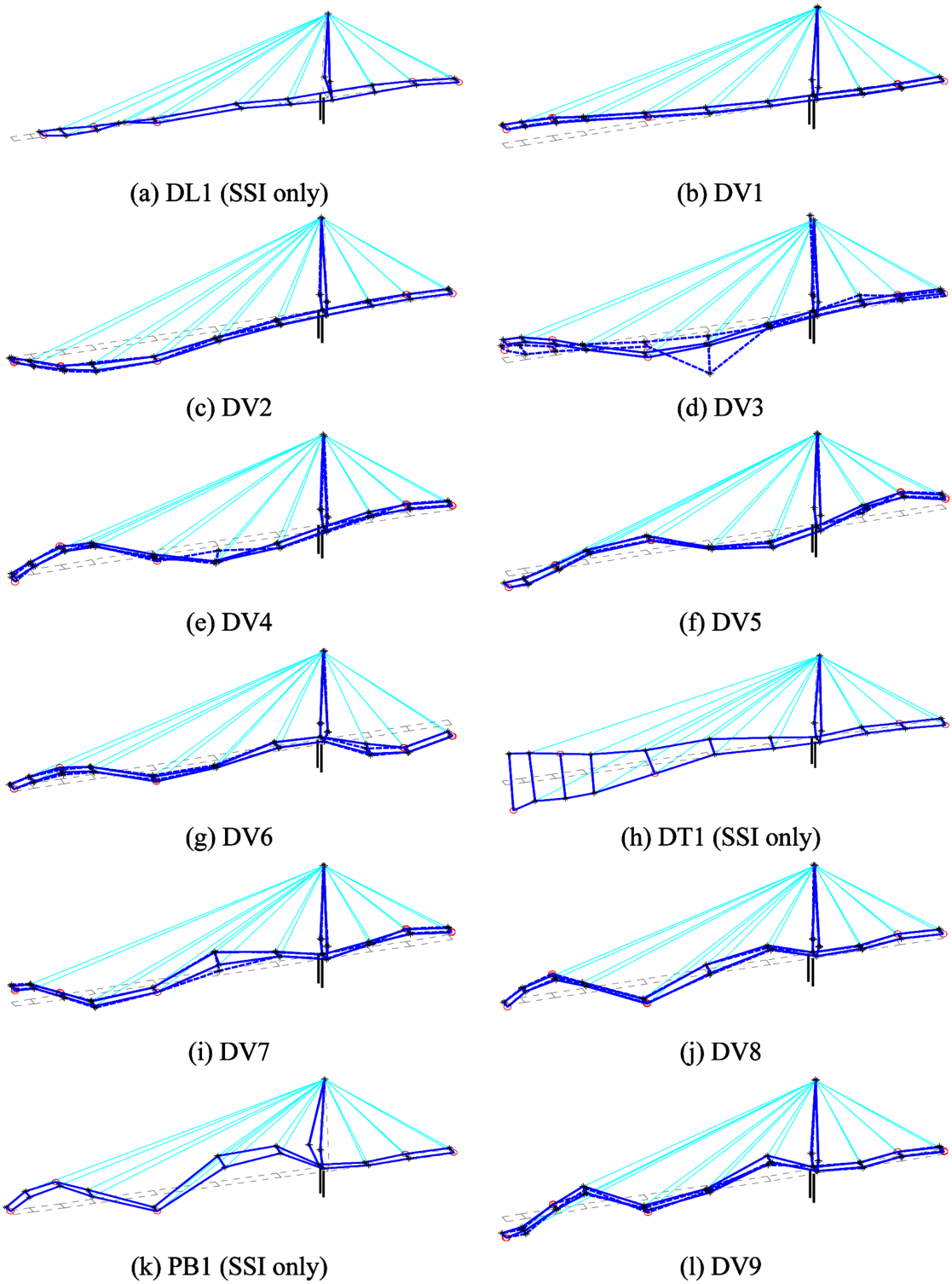

Fig. 11 Mode shapes from SSI (solid line) and FDD (dashed line): Jindo-side, on 9/11/2009

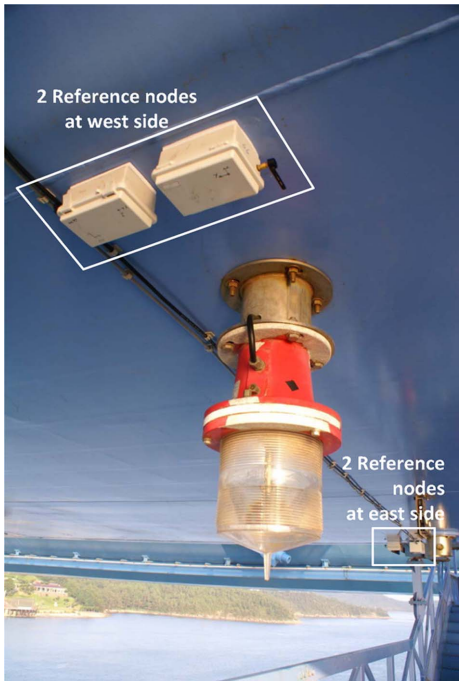

Fig. 12 Overlapped reference nodes installed on the Jindo Bridge

monitoring the cables are mounted approximately 3 m above the deck to facilitate access to the nodes; for this location, the rubber dampers do not affect significantly the response of the cable.

5.2 Vibration method for cable tension estimation

Given the importance of cables for the global integrity of a cable-stayed bridge, continuous monitoring of cable tension forces is prudent to assess cable degradation and anchorage slippage (Cho *et al.* 2010). In this study, the cable tensions are estimated using the identified natural frequencies. For this purpose, the tension force and the natural frequencies can be related as (Park *et al.* 2008)

$$\left(\frac{f_n}{n}\right)^2 = \frac{T}{4mL_{eff}^2} + \frac{EI\pi^2 n^2}{4mL_{eff}^4} = a + bn^2 \tag{9}$$

where T is cable tension force; n is the order of the dominant modes; f_n is the frequency of n-th dominant modes; m is unit mass of the cable; and L_{eff} is the effective length of the cable. A regression can be performed between $(f_n/n)^2$ and n^2 to obtain the intercept a and slope b in Eq. (9); subsequently, T can be determined as

$$T = 4mL_{eff}^2 a \tag{10}$$

Fig. 8 shows two examples of the measured acceleration data from on tri-axial accelerometers on the cables of Jindo side. Fig. 15 shows the Fourier amplitude spectra (FAS) for the cable motions along with the FAS for deck motions. Fig. 15 indicates that of the many peaks apparent in the FAS

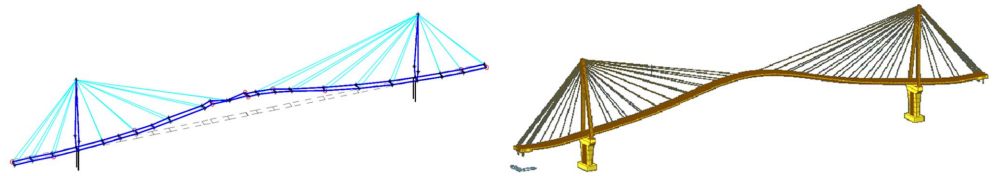

(a) DV1 (MAC: 0.957)

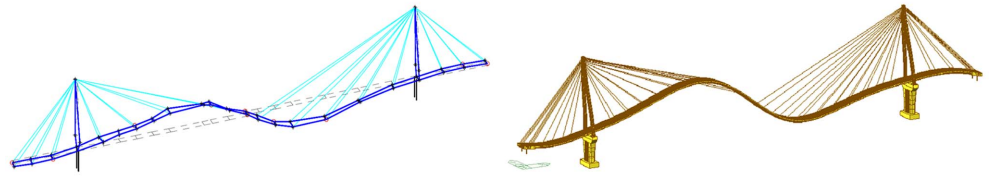

(b) DV2 (MAC: 0.986)

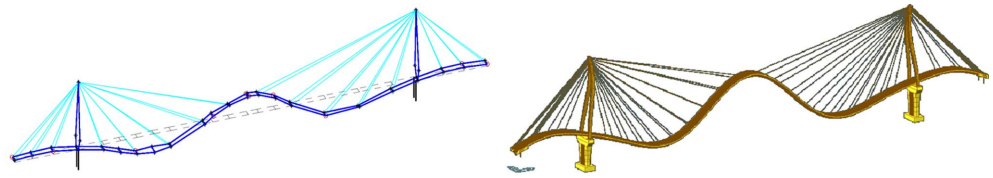

(c) DV3 (MAC: 0.975)

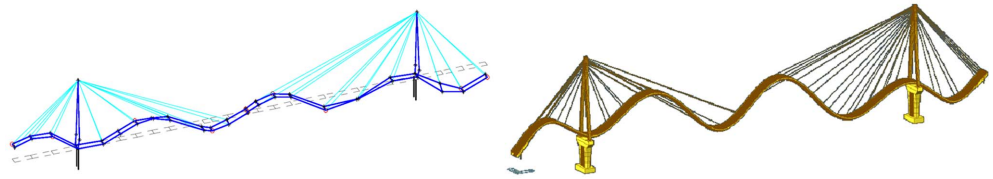

(d) DV6 (MAC: 0.949)

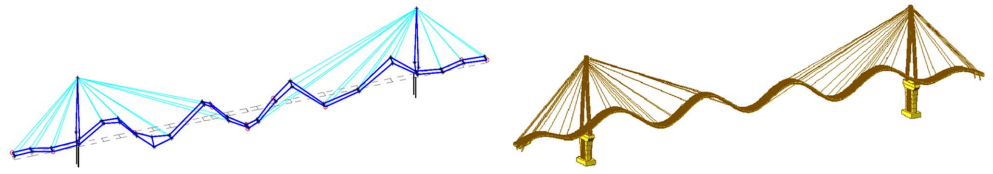

(e) DV9 (MAC: 0.943)

Fig. 13 Mode shapes identified from the data (left) and from the FE analysis (right)

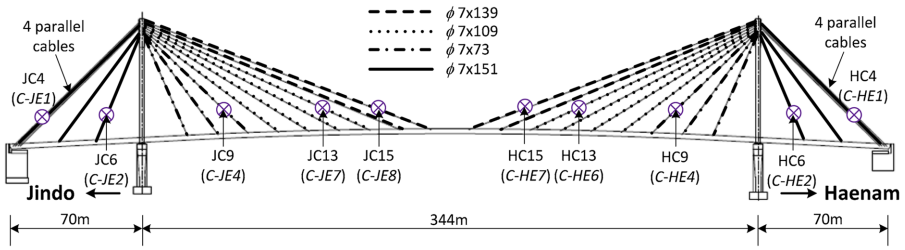

Fig. 14 Arrangement of stay cables and wireless sensors on cables (sensor numbers in parentheses)

for the vertical cable vibration, some can be associated with the deck motion owing to deck-cable interaction, particularly in the vertical direction.

Table 3 Properties of the cables monitored

Cables	HC4, JC4	HC6, JC6	HC9, JC9	HC13, JC13	HC15, JC13
Cable type	ϕ7×151	ϕ7×151	ϕ7×73	ϕ7×109	ϕ7×139
Elasticity (tonf/mm^2)	20.0	20.0	20.0	20.0	20.0
Area (mm^2)	5811.0	5811.0	2809.0	4195.0	5349.0
Length (m)	97.10	65.00	83.17	141.76	174.15
Effective length (m)	95.38	63.33	79.01	136.87	169.69
Unit mass (ton/m)	0.00486	0.00486	0.00236	0.00354	0.00448
Design cable sag (mm)	256.0	96.0	221.0	537.0	809.0
Design tension force (tonf)	237.0	271.0	90.0	160.0	202.0
Allowable tension force (tonf)	470.0	470.0	227.0	339.0	433.0

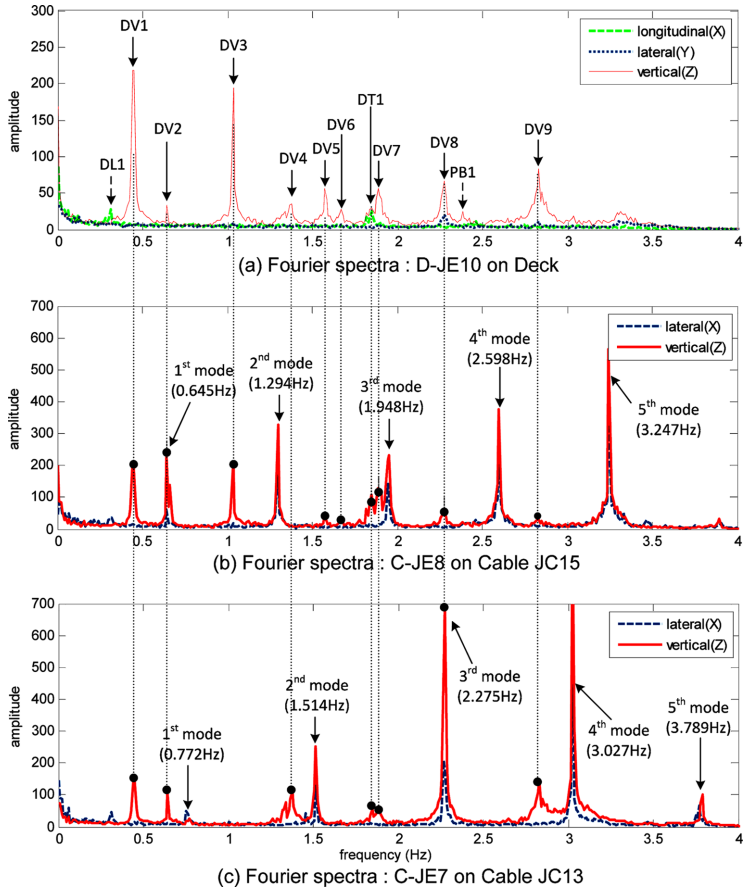

Fig. 15 Fourier spectra of acceleration data on the deck and cables (Jindo-side, on 9/11/2009)

However, the FAS for the lateral cable vibration do not contain so many peaks related to the deck motion. Because of the circular cross-section, slenderness and small sag of the stay cable, the modal properties of the cable are very similar in the vertical and lateral directions. Hence, in this study, the natural frequencies of the cables are extracted from vertical vibration with complementary use of

the lateral vibration components. The first five identified frequencies for two cables are: 0.645, 1.294, 1.948, 2.598, and 3.247 Hz for Cable JC15 with Node C-JE8, and 0.772, 1.514, 2.275, 3.027 and 3.789 Hz for Cable JC13 with Node C-JE7. The natural frequencies are found to be almost proportional to the order of modes (n), which is a dynamic characteristic of a slender cable with little bending and sag effect (Irvine 1981, Cho *et al*. 2010).

5.3 Interaction between deck and cables

Fig. 15 shows that the 1st frequency of Cable JC15 with Node C-JE8 is very close to the frequency of the 2nd vertical mode of the deck, while the 3rd frequency of Cable JC13 with Node C-JE7 is very close to the frequency of the 8th vertical mode of the deck. If the frequency of oscillation of the deck and/or tower falls in the neighborhood of the frequencies of the lower modes of a stay cable, the stay cable may be subjected to large vibration (Pinto da Costa *et al*. 1996). Such interaction between deck/pylon and cable vibration in the lower frequency range has been reported by Caetano *et al*. (2008) on the International Guadiana cable-stayed bridge in Portugal and by Weng *et al*. (2008) on the Gi-Lu cable-stayed bridge in Taiwan. This phenomenon, called as parametric excitation, is generally difficult to avoid in long-span bridges with many cables. However, if the cable vibration levels are found to be significant, cable dampers may be introduced to mitigate the response.

5.4 Estimated cable tension forces

Based on the identified dominant frequencies, the tension forces for the 10 cables are estimated as shown in Fig. 16. The estimated tension forces for the cables show consistency with respect to the monitoring periods. In Table 4, the averages of the estimated tension forces are compared with those obtained from two previous regular inspections in 2007 and 2008, as well as those from the

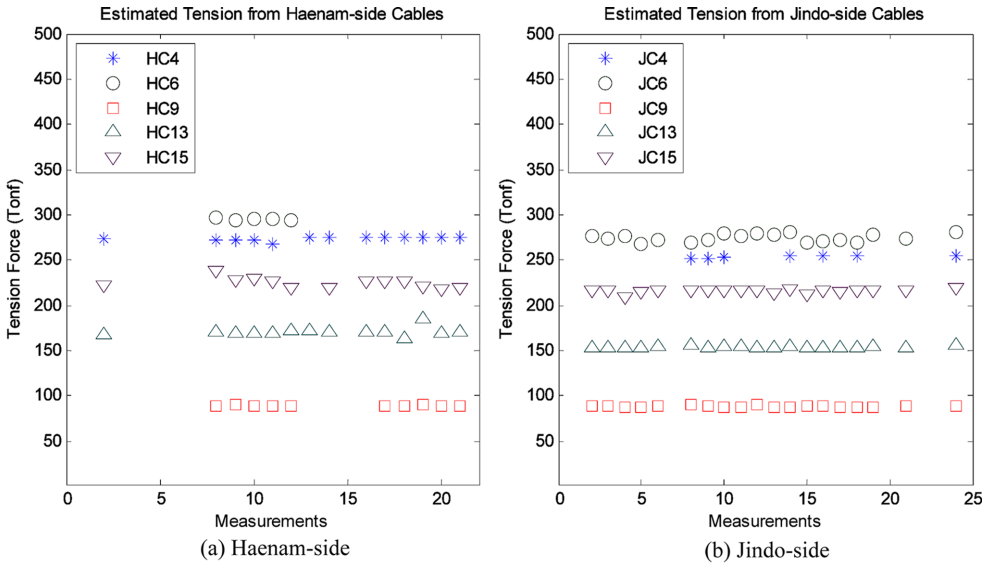

(a) Haenam-side (b) Jindo-side

Fig. 16 Estimated tension forces for 10 cables

Table 4 Comparison of estimated tension forces with those from previous regular inspections in 2007 and 2008

Cables (East-side)		Estimated tension forces (tonf)			Initial design values (tonf)	Maintenance thresholds (tonf)
		Present WSSNs in 2009 (averaged)	Previous inspections			
			in 2007	in 2008		
Haenam-side	HC4	274.0 (2.04)*	262.7	268.4	246.2	329
	HC6	294.7 (-3.19)*	304.6	304.1	271.8	329
	HC9	89.3 (0.90)*	86.9	88.5	87.6	158
	HC13	170.2 (3.00)*	164.0	165.1	163.6	237
	HC15	224.9 (2.18)*	219.9	220.0	204.8	303
Jindo-side	JC4	254.0 (1.30)*	245.1	250.7	245.9	329
	JC6	274.5 (-1.09)*	282.0	277.5	271.5	329
	JC9	88.5 (2.15)*	85.5	86.6	88.2	158
	JC13	154.3 (2.33)*	148.3	150.7	164.1	237
	JC15	216.8 (0.14)*	214.1	216.5	201.3	303

*The differences from regular inspection in 2008 are shown in the parentheses.

initial design, and those from the maintenance thresholds which are 60% of allowable tension forces of the cables (ATMACS 2008). The current estimations are found to be very close to the tension forces from two previous inspections with less than 4% difference. The tension forces of 8 cables have increased slightly with time, while those of 2 cables (HC6 and JC6) supporting the side spans have slightly decreased. The estimated cable tension forces are generally larger than the initial design values (10% at maximum) except JC13. All cable tension values are well within the maintenance thresholds, indicating that the cables are in safe operation.

6. Conclusions

This paper analysed the data collected from the 2nd Jindo Bridge, a cable-stayed bridge in Korea that is a structural health monitoring (SHM) international test bed for advanced wireless smart sensor network (WSSN) technology. A FE model of the bridge has been constructed based on its detailed drawings. Modal properties of the bridge were evaluated using two different output-only identification methods: FDD and SSI. Tension forces for 10 selected cables were also derived from the ambient acceleration data using a vibration method. The results of data analyses are summarized as follows:

1) Modal properties of the bridge were successfully determined from the ambient acceleration measurements obtained from the WSSNs using both FDD and SSI. The natural frequencies identified using the WSSNs were found to be in excellent agreement with those previously obtained using the existing wired sensors. The extracted mode shapes show excellent agreements with those from the FE analysis. SSI with high system order (larger than 60) is found to be very appropriate for extracting the modes without extensive amounts of data.

2) The frequencies of the higher modes of the FE model are found to differ from the identified values by less than 16%, which indicates the need for updating of the FE model.

3) The interaction between the deck and cables must be considered carefully to obtain accurate estimates of the natural frequencies of the cables, which are used for tension force estimation. To

this end, complementary use of the lateral vibration data of the cables was shown to be beneficial, because they are less sensitive to the deck motion.

4) The estimated tension forces for the 10 cables were very close to those from 2 previous regular inspections (i.e., less than 4% difference).

Finally, a substructural damage identification method for a cable-stayed bridge is now under development, with full utilization of the decentralized computing capabilities of the wireless smart sensor nodes. In this approach, substructural modal information for the deck/pylon and cable tension forces is combined to provide a comprehensive assessment of the structural integrity of the bridge.

Acknowledgements

This work was supported by the Korea Research Foundation Grant funded by the Korean Government (MEST) (NRF-2008-220-D00117), the National Science Foundation Grant CMS 06-00433 (Dr. S.C. Liu, Program Manager), and Smart Infrastructure Technology Center (SISTeC) at KAIST. Their financial supports are greatly appreciated. Additionally, cooperation of the Ministry of Land, Transport and Maritime Affairs in Korea, Daewoo Engineering Co. Ltd. and Hyundai Construction Co. Ltd. are gratefully acknowledged.

References

ATMACS (2008), *Consulting for the measurement systems for integrated entrusted management of long-span bridges (The 1st and 2nd Jindo Bridges) (in Korean)*, Sungnam, Gyunggi-do, Korea.

Brincker, R. Zhang, L. and Andersen, P. (2001), "Modal identification of output-only systems using frequency domain decomposition" *Smart Mater. Struct.,* **10**, 441-445.

Caetano, E., Cunha, A., Gattulli, V. and Lepidi, M. (2008), "Cable-deck dynamic interactions at the International Guadiana Bridge: On-site measurements and finite element modeling", *Struct. Control Health Monit.*, **15**(3), 237-264.

Cho, S., Lynch, J.P., Lee, J.J. and Yun, C.B. (2010), "Development of an automated wireless tension force estimation system for cable-stayed bridge", *J. Intel. Mat. Syst. Str.,* **21**(3), 361-376.

Ernst, J.H. (1965), "Der E-modul von seilen unter berucksienhtigung des durchanges (in German), *Der Bauingenieur*, **40**(2), 52-55.

Fujino, Y., Siringoringo, D.M. and Abe M. (2009), "The needs for advanced sensor technologies in risk assessment of civil infrastructures", *Smart Struct. Syst.*, **5**(2), 173-191.

Irvine, M. (1981), *Cable structures*, Dover Publications, Inc., New York, USA.

Jain, A., Jones, N.P. and Scanlan, R.H. (1998), "Effect of modal damping on bridge aeroelasticity", *J. Wind Eng. Ind. Aerod.*, **77**(8), 421-430.

Jang, S., Jo, H., Cho, S., Mechitov, K., Rice, J.A., Sim, S.H., Jung, H.J., Yun, C.B., Spencer, Jr., B.F. and Agha, G. (2010), "Structural health monitoring of a cable stayed bridge using smart sensor technology: deployment and evaluation", *Smart Struct. Syst.*, **6**(5-6), 439-459.

Jeong, M.J. and Koh, B.H. (2009), "A decentralized approach to damage localization through smart wireless sensors," *Smart Struct. Syst.,* **5**(1), 43-54.

Koo, K.Y., Lee, J.J., Yun, C.B. and Kim, J.T. (2008), "Damage detection in beam-like structures using deflections obtained by modal flexibility matrices", *Smart Struct. Syst.*, **4**(5), 605-628.

Koshimura, K., Tatsumi, M. and Hata, K. (1994), "Vibration control of the main towers of the Akashi Kaikyo Bridge", *Proceedings of the 1st World Conference on Structural Control*, Los Angeles, California, USA.

Li, H., Liu, M., Li, J.H., Guan, X.C. and Ou, J.P. (2007), "Vibration control of stay cables of the Shandong Binzhou yellow drive highway bridge using magnetorehaological fluid dampers", *J. Bridge Eng.*, **12**(4), 401-409.

MidasIT (2009), http://www.midasit.com.
Overschee, P.V. and De Moor, B. (1993), "Subspace algorithms for the stochastic identification problem", *Automatics*, **29**(3), 649-660.
Pakzad, S.N., Fenves, G.L., Kim. S. and Culler, D.E. (2008), "Design and implementation of scalable wireless sensor network for structural monitoring", *J. Infrastruct. Syst.*, **14**(1), 89-101.
Park, Y.S., Choi, S.M., Yang, W.Y., Hong, H.J. and Kim, W.H. (2008), "A study on tension for cables of a cable-stayed bridge damper is attached (in Korean)", *J. Korean Soc. Steel Constr.*, **20**(5), 609-616.
Peeters, B. and De Roeck, G. (1999), "Reference-based stochastic subspace identification for output-only modal analysis", *Mech. Syst. Signal Pr.*, **13**(6), 855-878.
Pinto da Costa, A., Martins, J.A.C., Branco, F. and Lilien, J.L. (1996), "Oscillations of bridge stay cables induced by periodic motions of deck and/or towers", *J. Eng. Mech.-ASCE*, **122**(7), 613-622.
Rice, J.A., Mechitov, K., Sim, S.H., Nagayama, T., Jang, S., Kim, R., Spencer, Jr., B.F., Agha, G. and Fujino, Y. (2010), "Flexible smart sensor framework for autonomous structural health monitoring", *Smart Struct. Syst.*, **6**(5-6), 423-438.
Sim, S.H., Carbonell-Marquez, J.F. and Spencer, Jr., B.F. (2010), "Efficient decentralized data aggregation in wireless smart sensor networks," *Proceedings of the SPIE conference on Sensors and Smart Structures Technologies for Civil, Mechanical and Aerospace Systems,* San Diego, CA, USA.
Weng, J.H., Loh, C.H., Lynch, J.P., Lu, K.C., Lin, P.Y. and Wang, Y. (2008), "Output-only modal identification of a cable-stayed bridge using wireless monitoring systems", *Eng. Struct.,* **30**(7), 1820-1830.
Yi, J.H. and Yun, C.B. (2004), "Comparative study on modal identification methods using output-only information", *Struct. Eng. Mech.*, **17**(3-4), 445-466.
Yun, J. (2001), *Finite element model updating for cable-stayed bridge using ambient vibration (in Korean)*, Ph.D. Thesis, Seoul National University, Seoul, Korea.